A new route to gold nanoflowers

Ferenc Liebig[1], Ricky Henning[1], Radwan M Sarhan[2,3,4], Claudia Prietzel[1], Matias Bargheer[2] and Joachim Koetz[1] (ORCID)

[1] Institute for Chemistry, University of Potsdam, 14476 Potsdam, Germany
[2] Institute for Physics, University of Potsdam, 14476 Potsdam, Germany
[3] Chemistry Department, Faculty of Science, Cairo University, Cairo 12613, Egypt
[4] School of Analytical Sciences Adlershof (SALSA), Humboldt-Universität of Berlin, 10099 Berlin, Germany

E-mail: koetz@uni-potsdam.de

CrossMark

Abstract

Catanionic vesicles spontaneously formed by mixing the anionic surfactant bis(2-ethylhexyl) sulfosuccinate sodium salt with the cationic surfactant cetyltrimethylammonium bromide were used as a reducing medium to produce gold clusters, which are embedded and well-ordered into the template phase. The gold clusters can be used as seeds in the growth process that follows by adding ascorbic acid as a mild reducing component. When the ascorbic acid was added very slowly in an ice bath round-edged gold nanoflowers were produced. When the same experiments were performed at room temperature in the presence of Ag^+ ions, sharp-edged nanoflowers could be synthesized. The mechanism of nanoparticle formation can be understood to be a non-diffusion-limited Ostwald ripening process of preordered gold nanoparticles embedded in catanionic vesicle fragments. Surface-enhanced Raman scattering experiments show an excellent enhancement factor of $1.7 \cdot 10^5$ for the nanoflowers deposited on a silicon wafer.

Supplementary material for this article is available online

(Some figures may appear in colour only in the online journal)

1. Introduction

The size- and shape-dependent optical properties of gold nanoparticles are of special interest in different fields of catalysis [1], photonics [2], sensing [3], and for biomedical uses [4, 5]. In particular, asymmetric gold nanoparticles, such as nanorods [6], nanocages [7], nanopyramids [8], nanotriangles [9] and nanoprisms [10] offer great potential in biomedical applications such as photothermal cancer therapy [11] and imaging [12] due to their absorption in the near-infrared (tissue diagnostic window) range [13]. Furthermore, the localized surface plasmon resonance can be easily tailored by small changes to the morphology [9, 14, 15]. The presence of the sharp tips and spikes of those anisotropic particles leads in surface-enhanced Raman scattering (SERS) to an increased electromagnetic field, which enhances the Raman signal and enables the investigation of catalytic reactions [15–18]. Studies of facet-dependent catalytic activity showed that high-index faceted particles aid molecule adsorption and are most active for surface reactions [18, 19]. Thus, the more exotic nanostars turned into the focus of the relevant research [20, 21].

Various protocols have been reported to produce anisotropic metal nanoparticles. Template-based strategies [22, 23] and seed-mediated routes [24, 25] have been used. The procedure used most often is to obtain asymmetric particles based on a seed-mediated, two-step process in the presence of the cationic surfactant cetyltrimethylammonium bromide (CTAB) [24]. In the second step, the CTAB-based gold seeds are grown by adding ascorbic acid (AA) in the presence of silver ions. Nevertheless, for the synthesis of nanostars a modified procedure is needed, e.g., by performing the seed-mediated growth process in a concentrated dimethylformamide solution in the

presence of poly(vinyl pyrrolidone) (PVP) [21]. A surfactant-free synthesis of gold nanostars using citrate-based seeds was reported by Yuan *et al* [26]. In that case, the AA has to be added quickly in the presence of silver ions. Under defined pH conditions the presence of Ag^+ ions is necessary for the formation of nanostars [26].

Recently, we have shown that flat gold nanotriangles are formed in a multivesicular Bis(2-ethylhexyl) sulfosuccinate sodium salt (AOT)/phospholipid-based template phase [27, 28]. The mechanism of the one-step formation process can be described by a diffusion-limited Ostwald ripening on the periphery of soft gold nanoparticle aggregates [29]. The resulting nanoplatelets, separated from spherical particles by a polyelectrolyte/micelle-based depletion flocculation [28], are long time stable with special optical and vibratory properties [30]. Ultrathin nanotriangles deposited in large scale close-packed monolayers on Si wafers can be successfully used as a substrate for monitoring photocatalytic reactions by SERS [31].

In the present work, we tried to synthesize gold nanoparticles in another type of vesicular template phase. It is already well known that mixtures of oppositely charged surfactants can form different types of organized systems, including vesicles [32]. For example, AOT builds spontaneously unilamellar vesicles with the cationic surfactant benzyl-n-hexadecyldimethylammoniumchloride, which are of special relevance in the areas of pharmacology, cosmetics, and foods [33, 34]. CTAB can form vesicles with sodium dodecylsulfate (SDS) and AOT, too [35, 36], but to the best of our knowledge this kind of vesicle has not yet been used as a template phase for making gold nanoparticles. CTAB is well-known as a shape-directing agent for the seed-mediated synthesis of gold nanorods showing a high reproducibility [25, 37, 38]. By forming a bilayer, CTAB interacts with the gold nanoparticle surface as well as Au ions in the solution [39]. Thereby, the CTAB counterion bromide plays a key role in the formation of Au nanorods through adsorption onto the side facets of the seeds. Additionally, the long tail of the surfactant facilitates the anisotropic growth [40]. A further advantage is that a CTAB bilayer prevents aggregation, leading to more stabilized particles [41].

Surprisingly, our first experiments have shown that AOT/CTAB-based vesicles, in the absence of additional components, can reduce a gold chloride solution in contrast to the surfactant components alone. This is another example showing that mixtures of oppositely charged surfactants may have synergistic benefits in their properties and applications [42]. However, the nanoparticle formation process is terminated at very small particle dimensions on the gold cluster level. Therefore, we started to use the gold clusters as a new type of seed for the formation of anisotropic gold nanoparticles by adding a mild reducing agent, i.e., AA. By varying the reaction temperature or adding silver ions, spiked gold nanostars with a flower-like inner structure and special optical properties can be synthesized.

2. Experimental details

2.1. Materials and methods

Tetrachloroauric(III)acid ($HAuCl_4 \cdot 3H_2O$), AOT and natrium borohydride ($NaBH_4$) were purchased from Sigma-Aldrich. CTAB was obtained from Fluka and AA from Roth. In all experiments, Milli-Q Reference A+ water was used.

UV–vis absorption experiments were performed with a Shimadzu UV–2600 spectrophotometer. Light microscopic images were captured and analyzed by the Leica DMLB microscope. Transmission electron microscope (TEM) micrographs were obtained by using a JEM-1011 (JEOL) TEM at an acceleration voltage of 80 kV as well as a JEM-2200 FS (JEOL) at 200 kV for high resolution (HRTEM). Scanning electron microscopic (SEM) investigations were performed with a S-4800 from Hitachi. Dynamic light scattering (DLS) and zeta potential measurements were made with a Malvern Nano Zetasizer 3600. A confocal Raman microscope (alpha 300, WITec, Ulm, Germany) was used to record Raman spectra of the samples. The microscope was equipped with an excitation laser at a wavelength of 785 nm and the laser beam was focused through a $100\times$ microscope objective. The spectra were recorded with a thermoelectrically cooled charge-coupled device detector (DU401A-BV, Andor, UK) placed behind the spectrometer (UHTS 300; WITec, Ulm, Germany) with a spectral resolution of $3\,cm^{-1}$. The Raman band of a silicon wafer at $520\,cm^{-1}$ was used to calibrate the spectrometer.

2.2. Vesicle formation and nanoparticle formation

A 0.16 M aqueous AOT solution and a 0.1 or 0.01 M CTAB solution were mixed together to obtain an AOT/CTAB vesicle solution. The turbid dispersion was agitated by using an ultrasound finger. The resulting vesicular dispersion (template phase) was characterized by light microscopy and DLS.

The vesicular template phase was mixed with a 2 mM gold chloride ($HAuCl_4$) precursor solution at a mixing ratio of 1:3. The obtained aqueous 'seed' solution was characterized by UV–vis spectroscopy and TEM microscopy.

Reducing components, i.e., citric acid, $NaBH_4$ or AA were added to the 'seed' solution by varying the temperature, the rate of adding the reducing agent and the molar ratio of the components. The resulting colored gold dispersions were characterized by UV–vis spectroscopy and TEM microscopy.

2.3. SERS substrates

For the layer formation of gold nanoflowers, a droplet of the dispersion was set on the Si substrate. By adding an ethanol-toluene mixture in a ratio of 5:1 to the droplet, the particles build a shimmering film on the interface, which remains as a layer after solvent evaporation. The silicon wafer fabricated with gold nanoflower film was immersed in a 1 mM aqueous
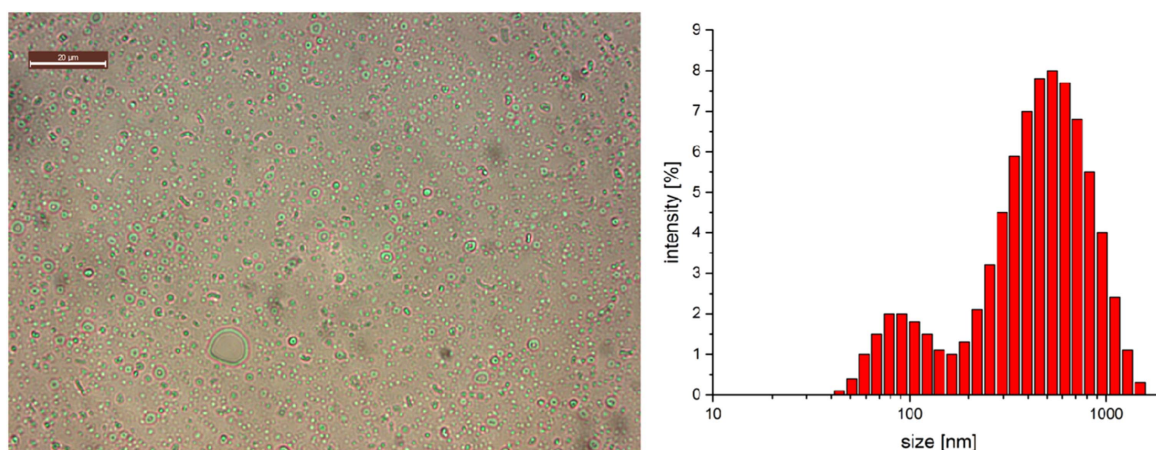
Figure 1. Light microscopic image of the vesicular template phase and the corresponding dynamic light scattering (DLS) plot.

3. Results and discussion

By mixing adequate amounts of the 0.1 M CTAB solution with the 0.16 M AOT solution, the vesicle phase is formed after sonification. The resulting light microscopic image (figure 1) show well-distributed vesicles in a size range between 100 nm and 5 μm. The giant vesicles (GVs) in the μm range are surrounded by a shell, similar to the SDS/CTAB-based catanionic vesicles obtained by Tah *et al* [35]. DLS measurements reveal a bimodal size distribution on the nanometer scale, with a small vesicle (SV) fraction at about 85 nm and a second larger vesicle (LV) fraction at about 500 nm.

By adding a 2 mM HAuCl$_4$ solution (gold precursor solution) to the vesicle phase at volume rates of 3:1 and heating the mixtures for 45 min to 45 °C, a color change to yellow/orange can be observed. The UV–vis spectra show an UV absorption maximum at 380 nm and a shoulder between 450 and 500 nm (figure 2). Recently, we have shown by HRTEM and asymmetric flow field flow fractionation (AFFFF) that gold clusters of diameter $\leqslant$ 2 nm show an absorption maximum at 360 nm [43]. Thus, it can be assumed that very small gold clusters are formed.

The corresponding TEM micrograph of the SV fraction is shown in figure 3(A). By zooming into such a vesicle, individual gold nanoparticles in the size range between 2 nm and 5 nm can be detected at higher magnification (figure 3(B)). The gold cluster, well embedded into the vesicular template phase, with particle diameter $\leqslant$ 2 nm, corresponds to the UV–vis absorption at 380 nm, and the individual and somewhat larger particles (around 5 nm in size) correspond to the UV–vis shoulder at 450–500 nm (compare with figure 2).

Astonishingly, our results show that the AOT/CTAB-based catanionic unilamellar vesicles reduce a gold precursor solution in the absence of any additional reducing component. It has to be mentioned that neither of the surfactant
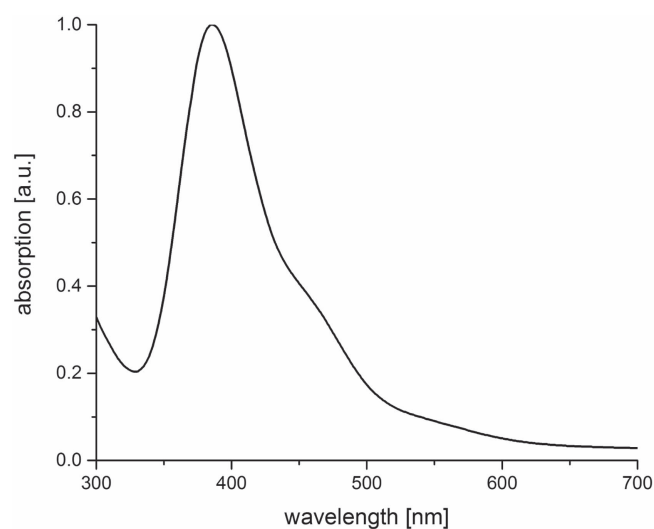

Figure 2. UV–vis spectra of the gold cluster 'seed' solution.

components, the CTAB solution or the AOT solution, can on its own reduce the gold chloride solution. Accordingly, electrostatic interactions between the functional head groups in the double layer are responsible for the reducing properties of the vesicular template phase. Due to the low reducing power accompanied by the template effect of the vesicles, the growth of gold crystals is already terminated at the cluster level. This interesting feature of the catanionic vesicles opens a door to the use of these gold clusters as 'seeds' for the seed-mediated synthesis of anisotropic gold nanoparticles.

Taking into account that there is still an excess of non-reduced Au^{3+} ions, we added three different reducing agents to our gold clusters embedded in the vesicular template phase, i.e., sodium borohydride, sodium citrate, and AA, respectively.

By using the strong reducing components NaBH$_4$ or sodium citrate, an optical color change to red and a spectroscopic shift of the cluster peak from 380 nm to 550 nm can be observed. Through the stepwise addition of a 0.1 M sodium borohydride solution to the seed solution, a stepwise degradation of the absorption cluster peak at 350 nm and a
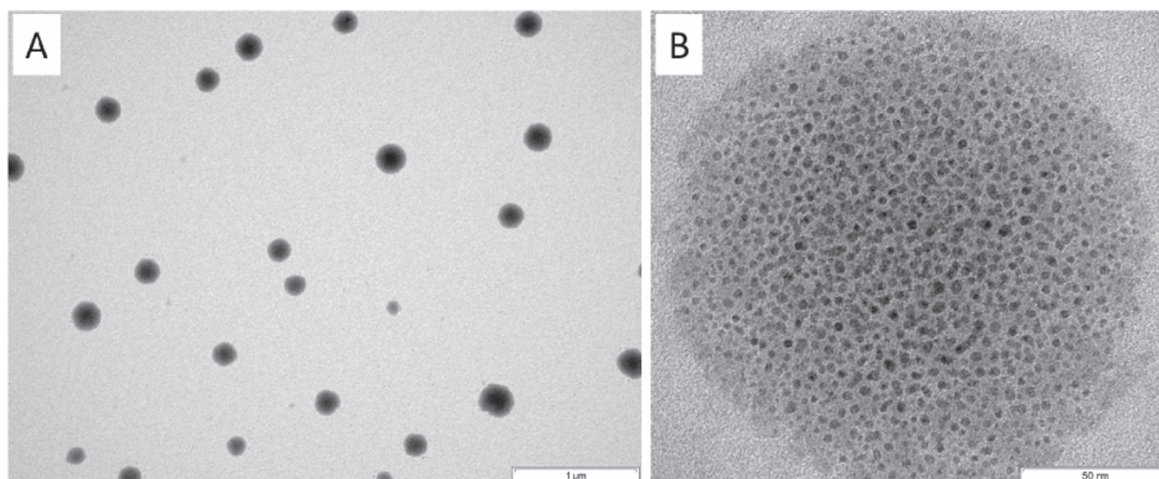
Figure 3. TEM micrographs of small vesicles after adding the gold precursor solution and heating the system to 45 °C for 45 min at lower (A) and higher (B) magnifications.
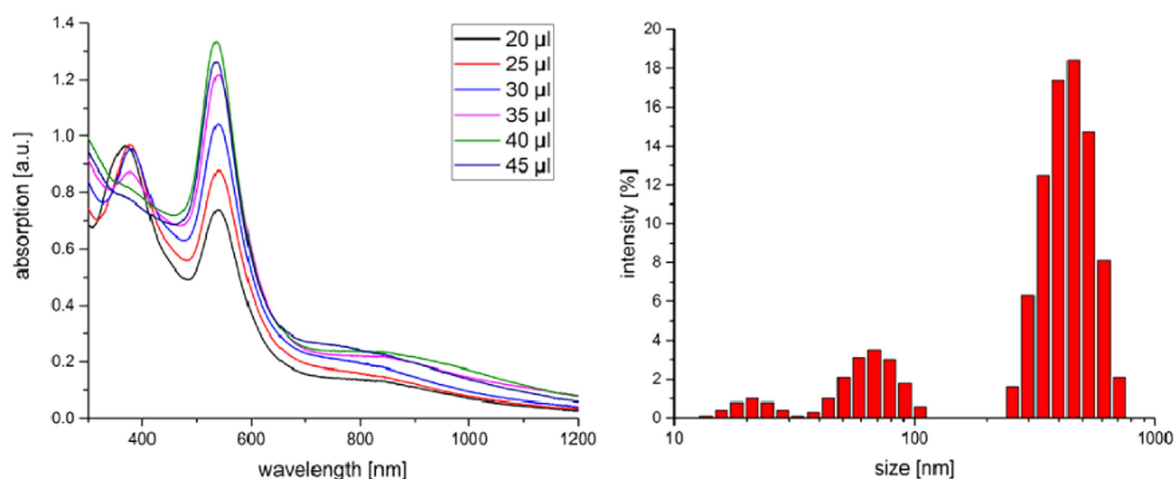

Figure 4. UV–vis spectra and DLS plot of the 'seed' solution after adding stepwise a 0.1 M ascorbic acid (AA) solution.
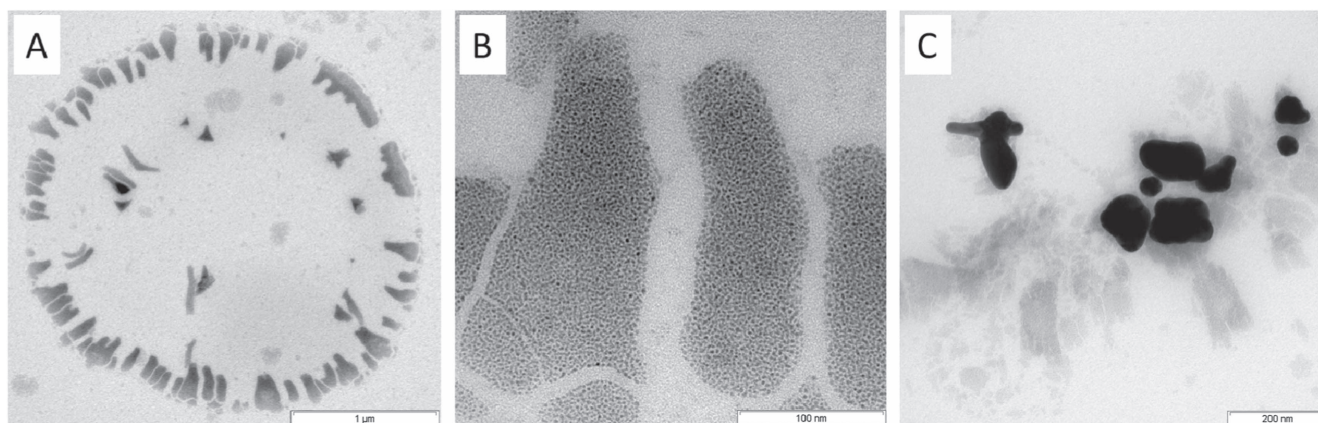

Figure 5. TEM micrograph of fragments of super large vesicles after adding stepwise a 0.1 M AA solution at room temperature (A); a magnified micrograph of the fragments with well-embedded small gold nanoparticles (B); and crystallized larger anisotropic gold nanoparticles (C).

corresponding increase of the surface plasmon resonance peak at 550 nm was noticed (figure S1 is available online at stacks.iop.org/NANO/29/185603/mmedia), which indicate the growth of gold clusters up to particle diameters ⩾ 5 nm [44]. When the same experiments were performed with AA, similar results were observed, but in addition to the peak at 550 nm a further broad peak between 800 and 1000 nm was detected (figure 4). After a dosage of 40 μl the cluster peak
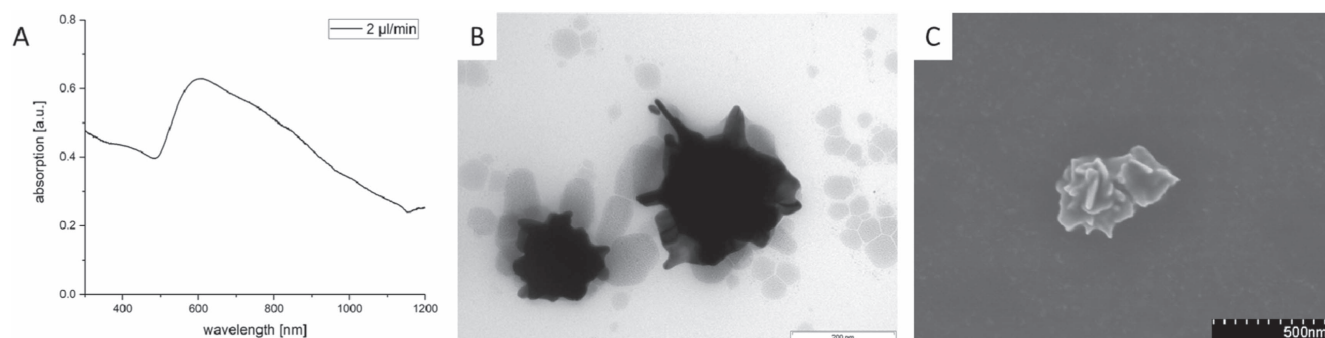
Figure 6. UV–vis spectra of the 'seed' solution after cooling in the ice bath and adding stepwise a 0.1 M AA solution with corresponding TEM and SEM micrographs of round-edged nanoflowers.

disappears and the UV maximum at 550 and 850 nm reaches a maximum. DLS experiments reveal a shift of the SV and LV peaks to smaller dimensions and the appearance of a new peak at about 20 nm. The peak shifts may be related to the decomposition of larger vesicles into fragments, and the new peak at about 20 nm to the formation of gold nanoparticles.

A corresponding TEM micrograph of the resulting system shows fragments of the GV template phase (figure 5(A)). A magnified picture of the irregular fragments (figure 5(B)) reveals well-embedded 5 nm sized gold nanoparticles, which are responsible for the UV absorption at 550 nm. Furthermore, anisotropic larger gold nanoparticles crystallize in the fragments (example shown in figure 5(C)), which seem to be responsible for the broad UV absorption in the near-infrared (NIR) range.

For a more controlled synthesis of such anisotropic gold nanoparticles, we varied the reaction conditions, i.e., the CTAB concentration was reduced to 0.01 M, the template was cooled in an ice bath, and the rate of silver nitrate addition was modified.

After cooling the 'seed' solution in an ice bath and adding the AA very slowly (2 μl/min), an UV absorption maximum between 580 and 620 nm (figure 6(A)) was observed. The corresponding TEM micrograph (figure 6(B)) shows spiked individual nanoparticles, which tend to aggregate at low temperatures (at 0 °C) and disaggregate at room temperature. In this case, a color change from blue to dark red can be observed. SEM micrographs show that round-edged nanoflowers or so-called nanostars are formed. It is noteworthy that the already well-established synthesis of spiked nanostars is performed at room temperature by the rapid addition of PVP-coated Au seeds to the gold chloride solution [21], or by the quick addition of a silver nitrate/AA solution to a citrate-stabilized seed solution [26]. In both cases, a fast addition at room temperature is realized, which is in contrast to our reaction conditions at low temperatures (0 °C) and slow addition rates.

It is already well known that Ag$^+$ ions are of special relevance by forming anisotropic gold nanoparticles in the second step of the seed-mediated synthesis, experimentally shown by the Liz-Marzan group [9, 20, 24]. Yuan *et al* have demonstrated that for the surfactant-free synthesis of nanostars, a fast addition of AA in the presence of Ag$^+$ ions is

required [26]. Nevertheless, the role of Ag$^+$ ions in shape-controlled synthesis is not entirely understood. Inspired by these results, further experiments focused on the role of Ag$^+$ ions in the crystallization process. Gold nanostars can be described as having a branched structure with a metal core and protruding sharp spikes [45, 46]. Therefore, we propose that the Ag$^+$ ions could specifically block the growth on the long sides, as observed for the nanorod growth in [38]. The formation of the spikes can thus be roughly compared to the growth of nanorods. In previous investigation related to CTAB-protected gold nanorods synthesis, the presence of Ag$^+$ ions generated a high yield of rod-shaped nanostructures with Au{110} faces on the side of the rods and {100} on the top of the rods. This can be explained by a selective silver adsorption to {110} Au facets inhibiting Au deposition on those surfaces, but allowing Au deposition on {100} surfaces [47].

By adding AA at the same rate in the presence of Ag$^+$ ions to the 'seed' solution, spiked nanoparticles are already formed at room temperature. The UV absorption curve becomes more distinct, with a maximum at 680 nm (figure 7(A)). SEM micrographs at a tilting angle of 45° offer a possibility to investigate the inner structure of the nanoparticles. Figure 7(B) shows that the spiked nanoparticles are supramolecular structured platelet aggregates with a flower-like inner structure; this means that sharp-edged nanoflowers are formed. Additional HRTEM measurement of a gold nanoflower tip shows a single crystallinity with ⟨101⟩ zone axis (figure 7(C)), quite similar to the tips of gold nanostars shown by Kumar *et al* [21].

Up to now, only a limited number of papers have reported the formation of gold nanoflowers (NFs) [48–54]. Rod-like gold nanoparticles [49–51] and sheet-like gold nanoparticles [52–54] can assemble into nanoflower superstructures. Winkler *et al* [54] discussed a time-dependent two-step model of autocatalytic growth, from sharp-edged to round-edged large micro-flowers, by using hydroxylamine as the reducing agent in a one-step procedure. Wang *et al* [52] discussed self-assembly of gold sheet structures due to Van der Waals and anisotropic hydrophobic attraction forces of sheet-like gold nanoparticles in the presence of PVP and Ag$^+$ ions.
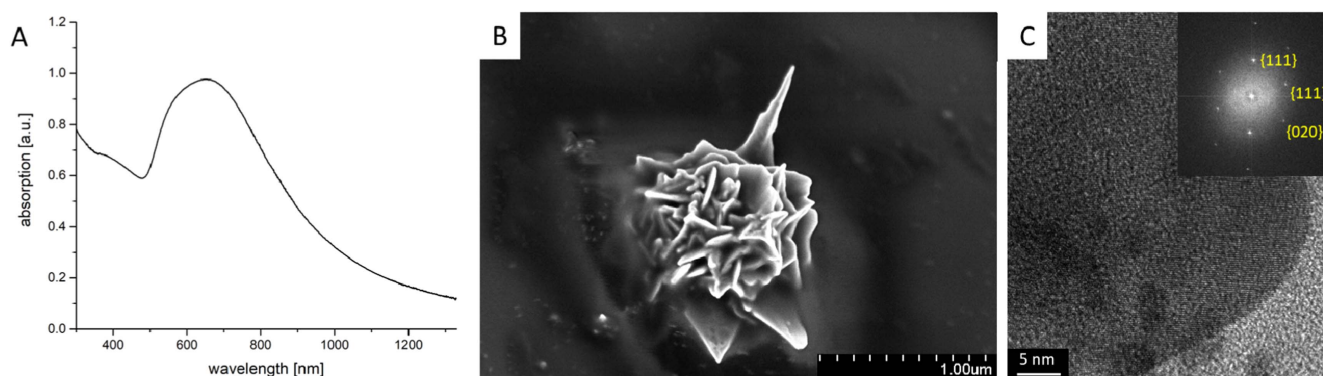
Figure 7. UV–vis spectra of the gold nanoflower dispersion with corresponding SEM micrograph and HRTEM micrograph (inset: fast Fourier transformation) of a spike of the sharp-edged nanoflowers formed at room temperature by slow addition of AA in the presence of Ag$^+$ ions.
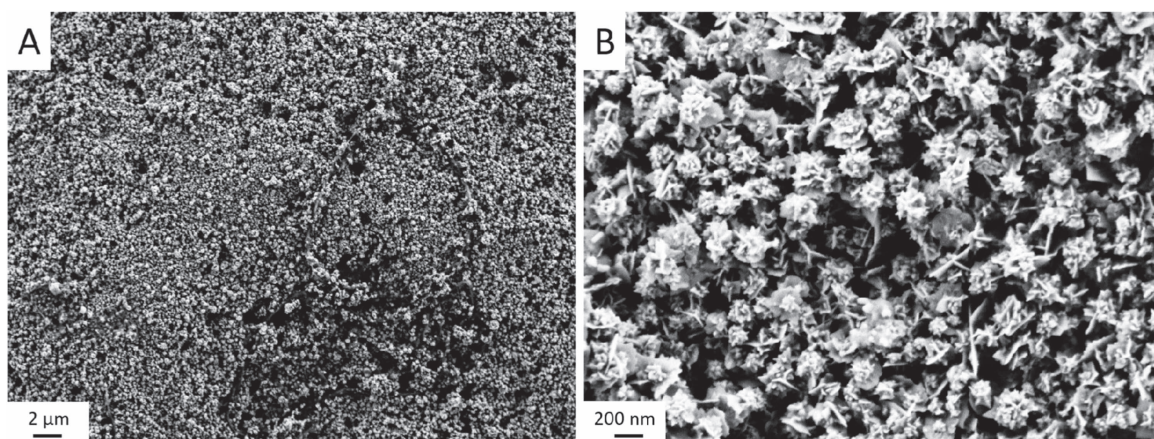

Figure 8. SEM micrograph of the gold nanoflower layer on Si substrate.

Symmetry-breaking properties of the Ag$^+$ ions attached to the gold nanoparticles embedded in the fragments seem to be responsible for the non-regular crystallization process in different directions to form curved nanoplatelets, which self-assemble to supramolecular flower-like nanoparticles. SERS experiments were performed to check the catalytic properties of these supramolecular formed NFs.

To investigate the performance in SERS, a droplet of the gold NF dispersion was set on a Si substrate. To avoid the coffee-ring effect and to obtain a close-packed layer of the nanoparticles, an ethanol–toluene mixture in a ratio of 5:1 was added to the droplet, as already detailed described in [31]. Thus, the nano-particles were transported to the interface and remain as a closely-packed layer after solvent evaporation (figure 8).

SERS has been used to provide 'fingerprint' information of the probed analyte, with higher sensitivity compared to conventional Raman scattering. Anisotropic nanoparticles such as gold nanotriangles and gold nanostars have been reported to show extraordinary SERS enhancement owing to their tips. These tips act as nanoantennas, at which the electromagnetic field and therefore Raman scattering is enhanced [55]. Herein, Rhodamine R6G was used to testify the SERS performance of the gold NFs. The gold NFs were deposited on silicon wafer and an uniform film was formed. Figure 9 shows the obtained SERS spectrum of R6G when
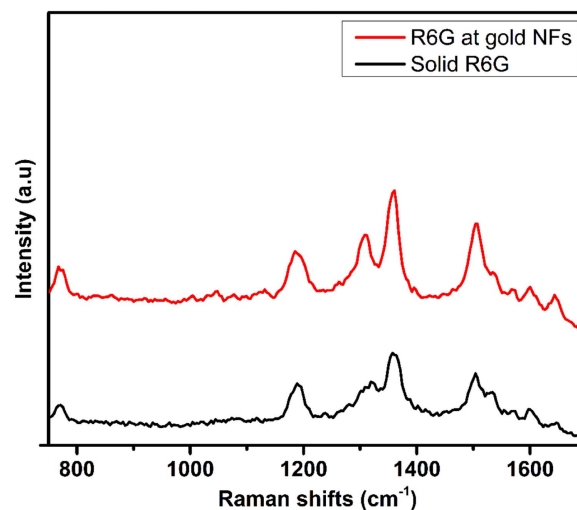

Figure 9. Surface-enhanced Raman scattering performance of the self-assembled gold nanoflowers and the bulk R6G molecules and the self-assembled gold nanoflowers.

the sample was immersed in a 1 mM aqueous solution of R6G. The SERS spectrum reproduced the characteristic Raman bands of the bulk R6G, where peaks at 1184 and 1307 cm^{-1} were assigned to the C-C and C-O-C stretching modes, respectively. The peaks at 1356 and 1504 cm^{-1} were

assigned to the aromatic ring C-C stretching modes of the R6G molecules [56].

The SERS enhancement factor (EF) of the NF film was estimated using the following equation:

$$EF = \frac{I_{SERS}}{I_{Raman}} \cdot \frac{N_{Raman}}{N_{SERS}}$$

where I_{SERS} and I_{Raman} are the intensities of a selected vibrational mode (vibrational mode at $1504\,cm^{-1}$) in the SERS and normal Raman spectra, respectively. N_{SERS} is the number of R6G adsorbed on the SERS substrate, while N_{Raman} is the number of the probed bulk R6G molecules. In this experiment, N_{SERS} and N_{Raman} were calculated to be $3.5 \cdot 10^5$ and $3 \cdot 10^{10}$, respectively. The SERS EF was estimated to be $1.7 \cdot 10^5$. Throughout the calculations, R6G molecules were assumed to form a monolayer on the gold NF substrate and each molecule was assumed to occupy $2.22\,nm^2$ of the illuminated area [57]. We attribute such high enhancement to the structure of the NFs, with many tips on their surfaces known as SERS hot spots, and to the nanogaps formed between these tips and their neighbors.

4. Conclusions

Catanionic vesicles are a new type of reducing agent for making gold clusters. The reduction process is terminated at the cluster level due to the templating effect of the catanionic vesicles. These gold clusters, with diameter $\leqslant 2\,nm$ and well embedded into catanionic vesicles, can be used as a 'seed' solution to form anisotropic gold nanoparticles. By adding AA as a mild reducing agent, the clusters grow to colloidal dimensions of about 5 nm in size. This process is accompanied by a fragmentation of the initially formed super large vesicles and the formation of larger anisotropic gold nanoparticles. The growth mechanism of the anisotropic gold nanoparticles in the catanionic vesicle fragments at low temperatures can be described by a non-diffusion-limited Ostwald ripening process, in contrast to the diffusion-limited Ostwald ripening process in solution, recently shown by our small angle x-ray scattering experiments [21]. At low temperatures (0 °C) and with a slow addition rate of AA, rounded-edged nanoflowers can be formed. In the presence of Ag^+ ions the crystallization process in the fragments can be further influenced, and flat nanoplatelets are formed, which self-assemble to sharp-edged nanoflowers at room temperature. The sharp-edged nanoflower superstructures deposited on a Si wafer show an excellent enhancement factor in SERS experiments, one order of magnitude higher than individual gold nanotriangles well ordered in a large scale close-packed monolayer, as shown by us earlier [23].

Acknowledgments

ORCID iDs

Joachim Koetz ● https://orcid.org/0000-0001-9113-1337

References

[1] Daniel M C and Astruc D 2004 *Chem. Rev.* **104** 293–346
[2] Millstone J E, Park S, Shuford K L, Qin L, Schatz G C and Mirkin C A 2005 *J. Am. Chem. Soc.* **127** 5312–3
[3] Frasca S, Rojas O, Salewski J, Neumann B, Stiba K, Weidinger I M, Tiersch B, Leimkühler S, Koetz J and Wollenberger U 2012 *Bioelectrochemistry* **87** 33–41
[4] Perrault S D, Walkey C, Jennings T, Fischer H C and Chan W C W 2009 *Nano Lett.* **9** 1909–15
[5] Duncan B, Kim C and Rotello V M 2010 *J. Control. Release* **148** 122–7
[6] Sau T K and Murphy C J 2004 *Langmuir* **20** 6414–20
[7] Skrabalak S E, Chen J, Sun Y, Lu X, Au L, Cobley C M and Xia Y 2008 *Acc. Chem. Res.* **41** 1587–95
[8] Lee J, Hasan W, Stender C L and Odom T W 2008 *Acc. Chem. Res.* **41** 1762–71
[9] Scarabelli L, Coronado-Puchau M, Giner-Casares J J, Langer J and Liz-Marzan L M 2014 *ACS Nano* **6** 5833–42
[10] Sun M, Ran G, Fu Q and Xu W 2015 *J. Exp. Nanosci.* **10** 1309–18
[11] Hirsch L R, Stafford R J, Bankson J A, Sershen S R, Rivera B, Price R E, Hazle J D, Halas N J and West J L 2003 *PNAS* **100** 13549–54
[12] Loo C, Lin A, Hirsch L R, Lee M H, Barton J, Halas N, West J and Drezek R 2004 *Technol. Cancer Res. Treat.* **3** 33–40
[13] Smith A M, Mancini M C and Nie S 2009 *Nat. Nanotechnol.* **4** 710–1
[14] Murphy C J and Jana N R 2002 *Adv. Mater.* **14** 80–2
[15] Jiang L, Tang Y, Liow C, Wu J, Sun Y, Jiang Y, Dong Z, Li S, Dravid V P and Chen X 2013 *Small* **9** 705–10
[16] Aldeanueva-Potel P, Carbo-Argibay E, Pazos-Perez N, Barbosa S, Pastoriza-Santos I, Alvarez-Puebla R A and Liz-Marzan L M 2012 *ChemPhysChem* **13** 2561–5
[17] Schlücker S 2014 *Angew. Chem., Int. Ed. Engl.* **53** 4756–95
[18] Zhang Q and Wang H 2014 *ACS Catal.* **4** 4027–33
[19] Burrows N D, Vartanian A M, Abadeer N S, Grzincic E M, Jacob L M, Lin W, Li J, Dennison J M, Hinman J G and Murphy C J 2016 *J. Phys. Chem. Lett.* **7** 632–41
[20] Barbosa S, Agrawal A, Rodriguez-Lorenzo L, Pastoriza-Santos I, Alvarez-Puebla R A, Kornowski A, Weller H and Liz-Marzan L M 2010 *Langmuir* **26** 14943–50
[21] Kumar P S, Pastoriza-Santos I, Rodriguez-Gonzales B, Javier Garcia de Abajo F and Liz-Marzan L M 2008 *Nanotechnology* **19** 015606
[22] Scott R W, Wilson O M and Crooks R M 2005 *J. Phys. Chem. B* **109** 692–704
[23] Ding W, Lin J, Yao K, Mays J M, Ramanathan M and Hong K 2013 *J. Mater. Chem. B* **1** 4212–6
[24] Lohse S E, Burrows N D, Scarabelli L, Liz-Marzán L M and Murphy C J 2014 *Chem. Mater.* **26** 34–43
[25] Smith D K and Korgel B A 2008 *Langmuir* **24** 644–9
[26] Yuan H, Khoury C G, Hwang H, Wilson C M, Grant G A and Vo-Dinh T 2012 *Nanotechnology* **23** 075102
[27] Schulze N, Prietzel and Koetz J 2016 *Colloid Polym. Sci.* **294** 1297–304
[28] Liebig F, Sarhan R M, Prietzel C, Reinecke A and Koetz J 2016 *RSC Adv.* **6** 33561–8
[29] Liebig F, Thünemann A F and Koetz J 2016 *Langmuir* **32** 10928–35

[30] von Reppert A, Sarhan R M, Stete F, Pudell J, Del Fatti N, Crut A, Koetz J, Liebig F, Prietzel C and Bargheer M 2016 *J. Phys. Chem.* C **120** 28894–9

[31] Liebig F, Sarhan R M, Sander M, Koopman W, Schuetz R, Bargheer M and Koetz J 2017 *ACS Appl. Mater. Interfaces* **9** 20247–53

[32] Jönsson B, Jokela P, Khan A, Lindman B and Sadaghiani A 1991 *Langmuir* **7** 889–95

[33] Villa C C, Mayano F, Ceolin M, Silber J J, Falcone R D and Correa N M 2012 *Chem. Eur. J.* **18** 15598–601

[34] Villa C C, Correa N M, Silber J J, Mayano F and Falcone R D 2015 *Phys. Chem. Chem. Phys.* **17** 17112–21

[35] Tah B, Pal P, Mahato M and Talapatra G B 2011 *J. Phys. Chem.* B **115** 8493–9

[36] Tan C Y, Khoo K S, Radiman S, Rahman I A and Amari N F 2014 *Sains Malaysiana* **43** 623–8

[37] Alkilany A M, Nagaria P K, Hexel C R, Shaw T J, Murphy C J and Wyatt M D 2009 *Small* **5** 701–8

[38] Orendorff C J and Murphy C J 2006 *J. Phys. Chem.* B **110** 3990–4

[39] Bullen C, Zijlstra P, Bakker E, Gu M and Raston C 2011 *Cryst. Growth Des.* **11** 3375–80

[40] Xiong Y, Cai H, Wiley B J, Wang J, Kim M J and Xia Y 2007 *J. Am. Chem. Soc.* **129** 3665–75

[41] Nikoobakht B and El-Sayed M A 2001 *Langmuir* **17** 6368–74

[42] Dar A A, Rather G M, Ghosh S and Das A R 2008 *J. Colloid Interface Sci.* **322** 572–81

[43] Lemke K, Prietzel C and Koetz J 2013 *J. Colloid Interface Sci.* **394** 141–6

[44] Jana N R, Gearhart L and Murphy C J 2001 *Langmuir* **17** 6782–6

[45] Burt J L, Elechiguerra J L, Reyes-Gasga J, Montejano-Carrizales J M and Jose-Yacaman M 2005 *J. Cryst. Growth* **285** 681–91

[46] Cabrera-Trujillo J, Montejano-Carrizales J, Rodriguez-Lopez J, Zhang W, Velazquez-Salazar J and Jose-Yacaman M 2010 *J. Phys. Chem.* C **114** 21051–60

[47] Liu M and Guyot-Sionnest P 2005 *J. Phys. Chem.* B **109** 22192–200

[48] Kharisov B I 2008 *Recent Patents on Nanotechnology* **2** 190–200

[49] Jena B K and Raj C R 2007 *Langmuir* **23** 4064–70

[50] Jena B K and Raj C R 2008 *Chem. Mater.* **20** 3546–8

[51] Yang D-P, Liu X, Teng C P, Owh C, Win K Y, Lin M, Loh X J, Wu Y-L, Li Z and Ye E 2017 *Nanoscale* **9** 15753–9

[52] Wang L, Wei G, Guo C, Sun L, Sun Y, Song Y, Yang T and Li Z 2008 *Colloids Surf.* A **312** 148–53

[53] Wang T, Hu X and Dong S 2006 *J. Chem.* B **110** 16930–6

[54] Winkler K, Kaminska A, Wojciechowski T, Holyst R and Fialkowski M 2011 *Plasmonics* **6** 697–704

[55] De Aberasturi D J, Serrano-Montes A B, Langer J, Henriksen-Lacey M, Parak W J and Liz-Marzán L M 2016 *Chem. Mater.* **28** 6779–90

[56] Zhai W-L, Li D-W, Qu L-L, Fossey J S and Long Y-T 2012 *Nanoscale* **4** 137–42

[57] Liu J, Yang T, Li C, Dai J and Han Y 2015 *Sci. Rep.* **5** 14942